Acta Materialia 221 (2021) 117378

Contents lists available at ScienceDirect

Acta Materialia

journal homepage: www.elsevier.com/locate/actamat

Full length article

Mimicking Barkhausen noise measurement by *in-situ* transmission electron microscopy - effect of microstructural steel features on Barkhausen noise

Mari Honkanen[a,*], Suvi Santa-aho[b], Lasse Laurson[c], Nasser Eslahi[d], Alessandro Foi[d], Minnamari Vippola[a,b]

[a] Tampere Microscopy Center, Tampere University, P.O. Box 692, FI-33014 Tampere University, Finland
[b] Materials Science and Environmental Engineering, Faculty of Engineering and Natural Sciences, Tampere University, P.O. Box 589, FI-33104 Tampere University, Finland
[c] Computational Physics Laboratory, Faculty of Engineering and Natural Sciences, Tampere University, Tampere University, P.O. Box 692, FI-33014 Tampere, Finland
[d] Computing Sciences, Faculty of Information Technology and Communication Sciences, Tampere University, P. O. Box 553, FI-33104 Tampere University, Finland

ARTICLE INFO

Article history:
Received 25 March 2021
Revised 8 September 2021
Accepted 3 October 2021
Available online 13 October 2021

Keywords:
Barkhausen noise (BN)
Ferromagnetic
Electron backscatter diffraction (EBSD)
In situ transmission electron microscopy (TEM)
Magnetic domains
Steels

ABSTRACT

A relationship between microstructural steel features and an outcome of the Barkhausen noise (BN) measurement was studied. Two different microstructures, martensite and pearlite-ferrite were used. Commonly, BN is linked directly to the sample hardness. A BN outcome from both martensite and pearlite-ferrite was, however, similar even though martensite has three times higher hardness. To reveal the connection between microstructural features and BN, a typical industrial BN measurement was mimicked by *in-situ* transmission electron microscopy (TEM). Martensite needed higher field strength to move domain walls (DWs) than pearlite-ferrite. In martensite, DWs gathered to areas with high dislocation density. Fe_3C lamellae in pearlite were strong pinning sites. DWs perpendicular and parallel to martensite laths started to move with the same field strength value. In pearlite, DWs perpendicular to lamellae started to move before the parallel ones. The RMS envelope of ferrite-pearlite starts earlier than that of martensite due to soft ferrite. Magnetically harder pearlite probably caused “a tail” and the envelope ends almost at the same time with martensite. . Nevertheless, similar peak width values were found for both samples. Martensite and pearlite have a lot of strong pinning sites, dislocations and Fe_3C, respectively. Fe_3C density is not as high as dislocation density. Ferrite has strong pinning sites only at low incidence, but as known, huge BN information volume compared to martensite and pearlite. This resulted in the similar pulse count from martensite and ferrite-pearlite.

1. Introduction

An automated magnetic Barkhausen noise (BN) analysis is an important non-destructive testing (NDT) method in industry. The analysis involves the measurement of the BN signal induced in ferromagnetic material by an applied magnetic field. BN is generated from the motion of magnetic domain walls within a sample in the time-varying magnetic field. Microstructural features inhibit the movements of the domain walls leading to discontinuous changes in the magnetization, i.e. the BN signal.

In ferromagnetic materials, a magnetic domain structure is a sub-structure of the grain structure and is linked to the microstructure when the sample is in the external magnetic field. The generation of the magnetic domain morphology follows the principle of minimizing the energy of the structure. The domain formation in material is a complex process involving various minimization and counterbalance processes of different types of energies: a magnetostatic energy and exchange and magnetocrystalline energies linked to a domain wall energy [1]. Usually, the multidomain formation is preferred to minimize the energy but the subdivision to the smaller and smaller domains is also limited by the energy balance. In addition, the magnetostriction phenomenon and the sample material inhomogeneities (inclusions, precipitations, crystal boundaries, internal stresses etc.) have an influence on the domain

* Corresponding author.
E-mail address: mari.honkanen@tuni.fi (M. Honkanen).

https://doi.org/10.1016/j.actamat.2021.117378

size and structure. This energy minimization holds for the domain width and domain wall pinning to inclusions or voids as well [2]. For example, Beale et al. [3] reported that the domain structure formed a regular structure between the laths with splitting to 90° walls near interfaces in the martensitic structure. Whereas, the pearlitic structure contained domains parallel to the cementite lamellae [3].

In the actual BN measurement with the varying, applied magnetic field, domain walls move back and forth: domains with the orientation closest to the field, grow at the expense of domains with different orientation. In the increasing field, all domains become parallel to the field (a single domain) at a certain saturation point. When the field goes back to zero, domains do not go to their original state (residual magnetism). The microstructural details and stress will have their own effect on the domain wall movements. The motion is hindered by the microstructural features, referred as pinning sites such as grain boundaries, voids, precipitates, and areas of high dislocation density [4]. Whereas, it is stated that applied or residual stresses have influence on the domain ordering/alignment in the sample [2]. Thus, the BN signal is very sensitive to the sample microstructure and stresses. Quite commonly, BN is linked directly to the sample hardness, e.g. [5,6]. This seems to be valid in the simple cases with known microstructural state, but general drawback of the BN method is that the interpretation of the results is challenging because of the complexity of the method itself and the outcome signals. Even if the sample hardness and/or stress is typically related to the BN outcome, their relationship is not fully understood, and contradictory BN results exist (e.g. [7] for stress dependence) due to certain particular exceptions coming from the magnetic behavior.

Typically, industrial BN applications are using only one BN outcome parameter such as the plain root-mean-square (RMS) amplitude and due to this, misleading conclusions might be produced because many variables are affecting the outcome RMS. Aranas et al. [8] tried to find and separate the effect of microstructure, texture, and stress (applied or residual) from the BN signal. To highlight the complexity of the BN signal origins, they found that differences in the magnetic anisotropy (caused by stress and/or crystallographic texture) give different BN signals from the same material. In the literature, conflicting BN results, especially for pearlitic structures, are presented [4,9]. Nevertheless, many scientific articles have proved the capability of the BN method to evaluate microstructural features/variations, e.g. [10,11], however, the domain wall structure and movement verification of the hypotheses behind the assumptions have not been verified in all cases, e.g. [12]. As already pointed out, the magnetic response of steel is complex: different interactions and non-linear behavior, hysteresis behavior, and even the response to stress is not linear in all cases as shown in e.g. [7,13]. Some of the complexity comes from the fact that the magnetostriction coefficient is dependent both on the applied stress condition as well as the applied magnetic field (during the measurement) [1].

Generated domain structure according to the sample microstructure, stress state, and the strength and amount of the pinning sites determine the behavior of the domain walls and thus the detected BN outcome. This is the basis of how magnetic methods are used to characterize microstructures. However, pinning effects of various microstructural features are complicated. Franco et al. [9] pointed out that domain walls are three-dimensional. Therefore, certain defects may pin dislocations but not domain walls and other defects may pin both of them [9]. Therefore, all microstructural features have not the same influence on the domain wall motion and the obstacles can have different pinning strengths. Various estimations of pinning types and their effects have been gathered to Table 1. Cullity and Graham [1] pointed out that the greatest influence of pinning sites on the magnetic properties is when the pinning sites are non-magnetic or their size is similar to the domain wall thickness. It is well known that grain boundaries are effective pinning sites as the crystallographic orientation changes between the grains [4]. According to Jiles [14], one common pinning site is dislocations which are microscopic inhomogeneous volumes of material. In addition, the pinning of the domain walls by dislocations is significantly influenced by the dislocation density and the critical value of pinning force per their unit length. Moreover, the morphology of the obstacle can also influence the pinning strength (globular vs. lamellar) via the coercivity [4]. For example, Byeon and Kwon [15] noticed that lamellar cementite pins the domain walls more strongly than globular cementite. In addition, in the case of pearlite with alternating ferrite and cementite lamellae, these lamellae, i.e. phase boundaries, are known to harden material in a magnetic way [16]. Beale et al. [3] also noticed that the ferrite-pearlite boundaries are effective pinning sites.

Magnetic domains can be detected with various observation systems such as Bitter method, magnetic force microscopy (MFM), and transmission electron microscopy (TEM) with Lorentz mode [18]. Generally, a standard objective lens (OL) of TEMs generates a strong magnetic field (~2 T) saturating the magnetization of the sample [10,19–22]. In the Lorentz mode, the OL is turned off and a Lorentz lens, far from the sample, is used for imaging causing only a low magnetic field on the TEM sample enabling the imaging of the domain walls [20]. The Lorentz force deflects the electron beam travelling through the sample producing contrast to TEM images between the magnetic domains [21,23,24]. The OL can be used to generate a vertical magnetic field and its strength can be adjusted by controlling the excitation of the OL and the Lorentz lens can be used for imaging [23,25].

The fact is that a better understanding on how various factors influence on the BN outcome signal is needed. In our earlier study [26], we noticed that RMS values from the martensite and pearlite-ferrite samples were similar even though their microstructure is dissimilar, and martensite has three times higher hardness compared to pearlite-ferrite. In this study, to make the connection between microstructural features and BN clearer, the actual, typical industrial BN measurement was mimicked, and the domain wall motion was visualized in the TEM for martensite and pearlite-ferrite samples. Via combining the microstructural characterization and visualization of the domain wall motion with the RMS envelope measured from the same microstructures, we found microstructural features affecting the BN peak position, width, and height. Thus, fundamental understanding on how the microstructural features are manifested in the properties of the BN outcome signal was achieved. This deep knowledge on the microstructural correlations to the BN signal opens up new possibilities to utilize the BN method in novel industrial quality control applications.

2. Experimental

2.1. Material

Material used was industrially relevant low-alloyed steel CF53. It is widely used e.g. in the power transmission component industry and we have used this material in our previous studies. Jominy end-quench samples were prepared from CF53 according to the standard ISO 642. The total length of the sample was 100 mm and diameter 25 mm. The Jominy end-quench test consists of an austenitizing treatment at 920 °C with 55 min hold time followed by a water quenching to the other end of the sample. The heat treatment was carried out in a chamber furnace in normal atmosphere (air) with a carbon bed where the sample was covered with carbon powder to avoid decarburization. The sample surface was cleaned with citric acid bath before BN measurements. Different cooling rates within the sample produce various microstruc-

Table 1
Pinning site types and their effects on the domain wall motion.

Pinning site type	Effect on domain wall	Refs.
Non-magnetic pinning sites	"Most effect to pinning"	[1,17]
Fe_3C considered as non-magnetic pinning sites	"Strong effect"	[4]
Pinning site's size similar to domain wall thickness	"Strong effect"	[1]
Dislocations as microscopic inhomogeneous volumes of material	"Weak/strong depending on dislocation density"	[14]
Pinning site orientation (Fe_3C lamellae parallel to domain wall)	"Strongly pinned"	[3,4]
Grain boundaries where crystallographic orientation changes	"Effective"	[4]
Domain wall bending by pinning sites	"Strong pinning"	[14]

tural regions. These regions were determined, and one sample of the pure martensitic structure (the quench end) and ferritic-pearlitic structure (from 65 mm of the quench end) were chosen for the studies. Ferrite-pearlite consisted about 57% of the ferrite phase based on the ImageJ software image acquisition captured from scanning electron microscope (SEM) images. The cooling rate of the quench end containing martensite is referred as 500 °C/s whereas in the ferrite-pearlite end (65 mm from quench end) about 2 °C/s [27]. A hardness tester (M4C-250, EMCO-TEST, Austria) was used to measure surface hardness values with Rockwell C (HRC) for the ground areas of the martensite and pearlite-ferrite samples.

2.2. Micro- and domain structure

Microstructures of the martensite and pearlite-ferrite samples were studied by SEM (XL30, Philips, The Netherlands), by a field-emission SEM (FESEM, Ultraplus, Carl Zeiss AG, Germany) equipped with an electron backscatter diffraction (EBSD) system (Symmetry, Oxford Instruments, UK), and by a transmission electron microscope (TEM, JEM-F200, Jeol, Japan). SEM samples were prepared by a traditional metallographic method by grinding with 320- 4000 SiC papers and then by polishing with a 3 µm diamond suspension followed by etching with 4% Nital. FESEM-EBSD samples were prepared by grinding with 320–2000 SiC papers and then by polishing with 3 µm and 1 µm diamond suspensions. A final polishing was done with a colloidal silica polishing liquid. TEM samples were prepared by a standard way: machining 3 mm diameter discs (thickness < 100 µm) and then electropolishing (TenuPol, Struers, Denmark) the discs until perforation using a solution (-50 °C) of nitric acid in methanol (1:2).

A crystallographic information from the martensite and pearlite-ferrite samples was collected by the EBSD system also enabling a transmission Kikuchi diffraction (TKD) analysis using the TEM samples. The EBSD detector includes also forescatter diodes (FSD) giving images with an orientation contrast. In the EBSD measurements, the acceleration voltage of 15 kV and the step size of 0.1 µm were used. In the TKD analysis, the acceleration voltage of 30 kV and the step size of 0.015 µm were used. The EBSD and TKD data was collected by the AZtec software and processed using the CHANNEL5 software (both from Oxford Instruments, UK). In the EBSD and TKD results, a band contrast (BC) map shows the quality of the Kikuchi diffraction pattern for each measurement pixel: bright means that the pattern quality is good, and it can be indexed, and black signifies that the pattern quality is poor. The colors in the inverse pole figure (IPF) maps (z direction) correspond to the crystallographic orientations as indicated by a colored stereographic triangle. To determine dislocation information from the EBSD data, local misorientation maps were created. Strain (dislocations) causes the curvature of the crystal lattice resulting in local misorientations.

Domain walls in the samples were studied by TEM using an objective mini-lens instead of the standard OL to minimize the magnetic field in the sample area. The Fresnel mode, i.e. a defocused condition, was used: underfocused and overfocused images reveal domain walls (180°) as white or black lines.

2.3. Barkhausen noise measurements

BN measurements were carried out with a BN analyzer (Rollscan 350, Stresstech Oy, Finland). A commercial curved sensor (S5857) to fit the sample surface was used with 5 peak-to-peak voltage (vpp) and 125 Hz measurement frequency. Measurement sampling frequency was 2.5 MHz. The measurement direction was tangential to the Jominy sample. The measurements were collected from four different measurement lines around the Jominy sample. All measurements of both microstructures were taken from the unpolished surface so that there was no effect on the grinding, i.e. mechanically induced stresses. The detailed description of the measurements can be found from [26]. MicroScan software (Stresstech Oy, Finland) was used to capture and calculate the BN features. The features root-mean-square (RMS), peak position, and full width at half maximum (FWHM) were taken into analysis directly from the MicroScan software. Pulse count was determined from the raw signal as averaged pulse count per burst (averaged over 33 bursts, using for each experiment a threshold value of three times the standard deviation of the signal in the region of the minimum signal amplitude in between the bursts).

The BN measurement itself is two-parted: first, to apply the electromagnetic field and then, to pick-up the BN signals with another coil. The electromagnetic field produced by the magnetizing yoke of the BN sensor will decay exponentially due to eddy current damping into the depth direction to the surface. Several material and measurement parameters are affecting the electromagnetic skin depth δ. In the simplest case, it can be estimated with the equation: $\delta = \frac{1}{\sqrt{\pi f \sigma \mu_0 \mu_r}}$, where f is frequency, σ is conductivity, μ_0 is the permeability of vacuum, and μ_r is the relative permeability of the material [2]. For example, Moorthy et al. [28] discussed that sensor properties such as distance between the magnetizing pole pieces and sensitivity of the coils affect the BN measurement depth. Thus, the exact information depth calculation is challenging. Based on the studies by Moorthy et al., the measuring depth is approximately between 150 and 20 µm depending on the analysing frequency range of 20−1000 kHz [29]. Recently, Stupakov et al. [30,31] studied the reading depth of BN with different microstructures: martensite [30] and pure ferrite together with ferrite-pearlite [31]. In the case of hard materials with fine structure (martensite and pearlite), they noticed that with a classical sample-wrapping coils the reading depth was ~200 µm as expected. However, with industrial surface-mounted coils the depth was only ~50 µm. In the case of ferrite, the depth was ~200 µm with both type coils [30,31].

2.4. Visualization of BN measurement by in-situ TEM

The BN measurement was mimicked, and the domain wall motion was visualized by *in-situ* TEM. Domain walls were imaged by using the objective mini-lens and the standard OL was used as a

vertical source of the applied magnetic field. By controlling the excitation of the OL, the strength of the applied field was varied. The field strength was increased up to ~0.4 T as in the actual BN measurements and several magnetization loops were carried out. Presented magnetic field strength values are only rough estimations determined by supposing that the maximum excitation of the OL generates the field strength of ~2 T [19–22,25] and by assuming no hysteresis and linear response of the OL [19,25]. In this work, the idea was to compare two different microstructures and they were studied in the same way and thus, absolute magnetic field strength values were not so important. However, the idea in the *in-situ* TEM studies was similar to the actual BN measurements: the field strength was varied from ~0 T to above the saturation point and several magnetization loops were carried out. TEM images (Lorentz mode, underfocus) were recorded and constructed to videos. As the relative position of the object changes during acquisition, the recorded TEM images are inherently misaligned. Therefore, before the video construction, the TEM images were first automatically co-registered with the iterative multiscale method [32], and then histogram-equalized and gamma-corrected for a better comparative visualization. In this particular application of [32], the co-registration used as reference the temporal median of a contiguous subset of images, which is progressively extended as further images get registered; an additional weighting based on the structural features in the image was also included in the algorithm to make the co-registration more robust with respect to the significant content and contrast differences between images.

3. Results and discussion

3.1. Micro- and domain structure

The micro- and domain structure of the martensite sample is presented in Fig. 1. The FSD and SEM images and the BC map superimposed with IPF map (Fig. 1a–c) indicate a lath martensite microstructure; an average lath width being 0.2 μm determined by TEM and EBSD. Based on the BC map superimposed with a local misorientation map (Fig. 1d) and TEM (in-focus) images (Fig. 1e), a typical high dislocation density exists in most of the martensite laths. However, there are also blocks with a low local misorientation (Fig. 1d). Fresnel images (Fig. 1e) reveal that the domain walls exit both parallel and perpendicular to the martensite laths. The walls perpendicular to the laths, continue over the laths. A domain size varies significantly, for example very small domains are formed inside the ellipse in Fig. 1e. It seems that a lath size affects the domain size: thin laths and small domains, wider laths (slightly lower dislocation density) and larger domains. Dislocations seem to bend the domain walls and the lath boundaries have a lesser effect (Fig. 1e).

The microstructure and domain structure of the pearlite-ferrite sample is presented in Fig. 2. The FSD and SEM images and the BC map superimposed with IPF map (Fig. 2a–c) indicate ferrite grains and pearlite colonies which are a two-phased, lamellar structure composed of alternating layers of ferrite and cementite (Fe_3C). The size of the ferrite grains is 5.7 ± 3.7 μm determined by ImageJ software from the SEM images (100 grains). The width of ferrite layers varies between ~0.05 and 1 μm and that of cementite layers between ~0.01 and 0.5 μm determined from SEM and TEM images. Thin cementite lamellae were not indexed by EBSD. The BC map superimposed with a local misorientation map (Fig. 2d) and TEM images (Fig. 2e) indicate almost dislocation-free ferrite grains and slightly higher local misorientation in the pearlite grains. However, the amount of the local misorientation is negligible compared to the martensite sample (Fig. 1d). This is natural because martensite has three times higher hardness compared to pearlite-ferrite. Fresnel images (Fig 2e) reveal that the domain walls exist both parallel and perpendicular to ferrite and cementite lamellae in the pearlite colonies and a domain size varies. In the pearlite colonies, also very small domains were observed as in the martensite sample. The domain size in the ferrite grains was large.

3.2. BN measurement results

BN measurements were collected from the unpolished surface so that there was no effect from grinding induced residual stresses. Normally, the grinding has influence on the sub-surface layer creating mechanical abrasion and thus meaningful changes to the surface residual stresses at certain depth and therefore affecting the Barkhausen noise RMS levels. Whereas the unpolished surface without machining should provide mainly the information of what is the effect of the microstructural details on the gained BN signal. The comparison of the ground and unpolished surface BN results can be found from our earlier study [26]. In the case of martensite, it should be noted that the phase transformation procedure itself with volumetric change will produce type-2 residual microstresses.

The hardness (HRC) value, RMS, peak position, and peak width (FWHM) for the unpolished surfaces of the martensite region of the sample and pearlite-ferrite region are presented in Table 2. The BN features (RMS, peak position, FWHM) were captured from the MicroScan software. Four different measurement locations around the sample in both microstructural regions were averaged. Example RMS envelopes from two different measurement locations for both microstructures (averaged over 33 bursts for each measurement, not over all data presented in Table 2) computed using the envelope function of Matlab with the rms option and window size of 0.2 ms are presented in Fig. 3. The envelopes show minor deviations depending on the measurement location, nevertheless the typical characteristics of the microstructures are visible.

The general trend was that the RMS (Table 2) increased slightly as a function of distance from the quenched end for as-quenched measurement locations, i.e., from martensite to pearlite-ferrite. However, the difference of martensite and pearlite-ferrite structure is not as large as it could be if only the hardness values of the two structures are considered (martensite having more than three times higher hardness value compared to pearlite-ferrite).

A peak position (Table 2) of the RMS envelope is linked to the magnetic field strength that is required for domain walls to overcome the pinning obstacles [35]. Thus, the peak position is sensitive to the pinning strengths of the given type of barriers in the structure. In our study, the peak position (Table 2 and Fig. 3) for pearlite-ferrite indicated lower magnetic field strengths for the domain wall motion than for martensite. According to Davut and Gür [36], the martensitic structure causes only small domain wall displacements. For tempering effects, Blaow et al. [37] noticed that over tempering martensite would decrease the peak position as the carbide structure changes and the hardness decreases. Whereas, the peak position/stress dependence was not linear: both the higher applied tensile and compressive stress increased the peak position values [37]. Sahebalam et al. [11] also noticed the decreasing trend of the peak position with respect to the increasing tempering temperature.

Interestingly, the peak width value (Table 2) of the martensitic and pearlitic-ferritic structures was similar despite of the differences in their microstructure (Figs. 1 and 2). A BN voltage pulse peak width gives the information on the magnetic hardness [11]. Inaguma et al. [38] proposed that a spacing between individual pinning sites correlates to the peak width: a larger spacing of the pinning sites will lead to the increased peak width. Stewart et al. [39] referred the peak width to measure the range over the BN is spread and relating it to the steepness of the hysteresis loop. Whereas for tempering effects, Blaow et al. [37] noticed that over-tempering martensite structure would lead to the decrease

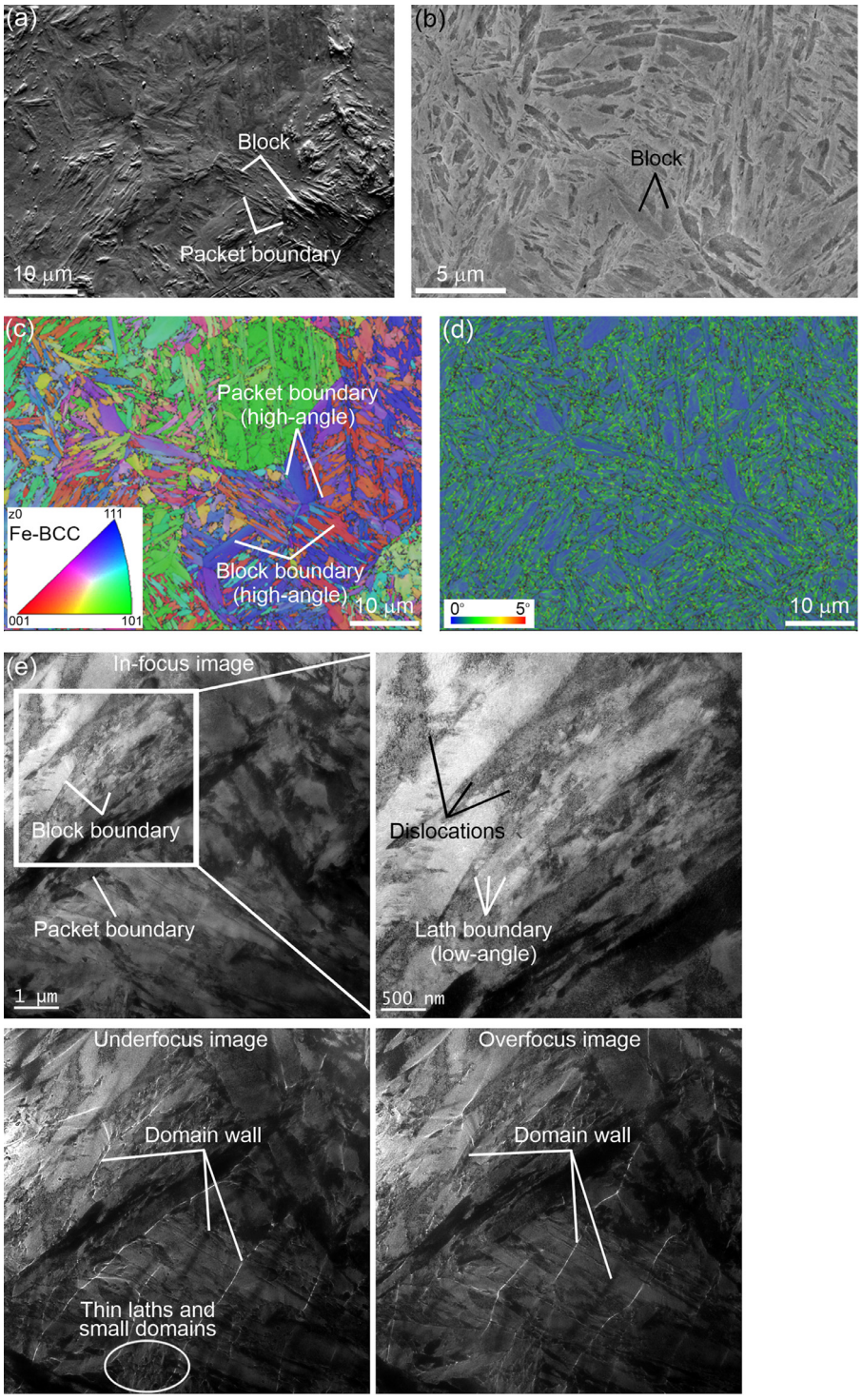

Fig. 1. Microstructure and domain structure of martensite sample, (a) FSD image, (b) SEM image (etched with 4% Nital), (c) BC map superimposed with IPF map, (d) BC map superimposed with local misorientation map and (e) two TEM images showing microstructure and Fresnel images showing domain walls.

Table 2
The hardness (HRC) values and BN features with standard deviations, i.e. RMS, peak position and peak width (FWHM) of the martensitic and pearlitic-ferritic structures.

	Hardness (HRC)	RMS [mV]	Peak position [a.u.]	Peak width (FWHM) [a.u.]
Martensite	56	248 ± 4.2	0 ± 0.8	42 ± 0.5
Pearlite-ferrite	16	268 ± 4.0	−33 ± 2.2	41 ± 2.2

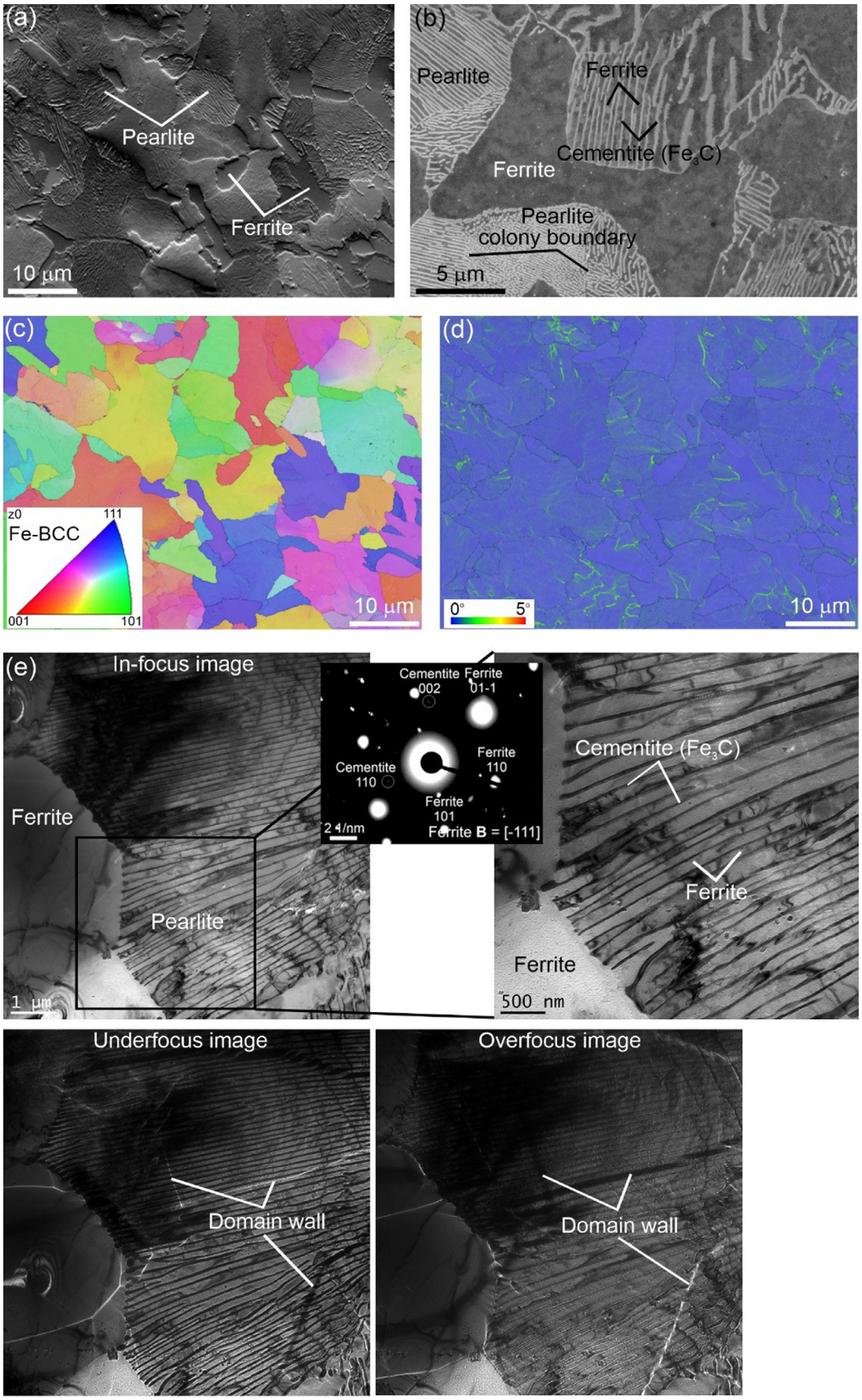

Fig. 2. Microstructure and domain structure of pearlite-ferrite sample, (a) FSD image, (b) SEM image (etched with 4% Nital), (c) BC map superimposed with IPF map, (d) BC map superimposed with local misorientation map and (e) two TEM images with selected area electron diffraction pattern (indexed based on [33,34]) showing microstructure and Fresnel images showing domain walls.

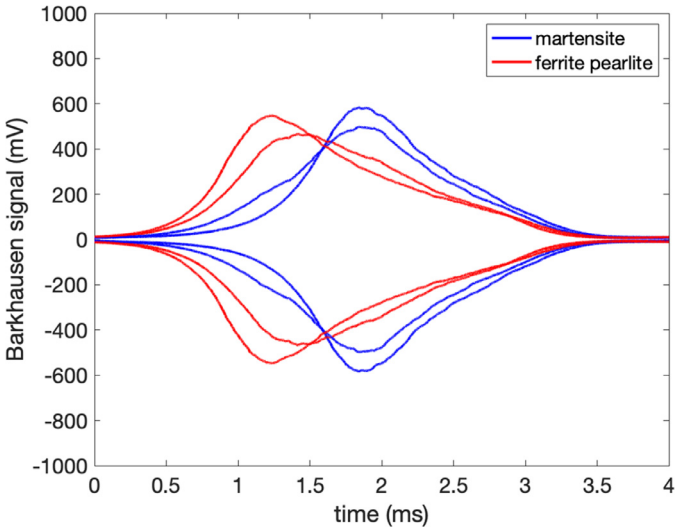

Fig. 3. Example RMS envelopes from two different measurement locations for martensite and ferrite-pearlite (note that Table 2 shows average BN features averaged over a larger set of measurements). Each of the four envelopes shown is averaged over 33 bursts.

of hardness and also decreased the peak width. Sahebalam et al. [11] also noticed this same decreasing trend of the peak width with respect to the increasing tempering temperature: quenched martensite has the highest width (domain walls overcome the obstacles in wider range of magnetic field) and further tempering of the structure decreased the peak width. Annealed structure containing ferrite-pearlite was referred as magnetically soft with the narrow peak width [11]. However, the observed surfaces of Sahebalam et al. [11] were machined so the effect of machining cannot be left out for the results. Blaow et al. [37] observed for stress effects that higher applied tensile stress causes the peak width value to increase and with increased applied compressive stress increases the peak width value also.

The pulse count was determined from the raw signals as averaged pulse count per burst, using a threshold as discussed above separately for each measurement (averaged over 33 bursts in each measurement, with the corresponding RMS envelopes shown in Fig. 3). This resulted in pulse counts of 517 and 539 for the two martensite measurements, and 530 and 589 for the two ferrite-pearlite measurements shown in Fig. 3, respectively (each mean value rounded to the nearest integer). Based on the literature, the pulse count can be related to how many separate pinning events occur: more hindrances to domain wall motion will create higher number of these individual BN events with smaller amplitude of them [14]. In our study, the pulse counts varied slightly from sample to sample and measurement to measurement, but overall were rather close for the two microstructures considered.

3.3. BN measurement mimicking by in-situ TEM

3.3.1. Martensite sample

Our empirical findings of practical BN measurements have indicated that the outcome of separate, actual BN measurements from martensite samples deviates and is not necessarily constant. During the *in-situ* TEM studies, we noticed that the behavior of the martensite sample varied from the magnetization loop to loop. For example, domain wall movements and saturation existed with different magnetic field strength values. The TEM images (in-focus and Fresnel images) at the initial stage, the BC map superimposed with IPF map from the same area collected by TKD technique, and a few Fresnel images (underfocus) from the same area showing the domain wall movements during one magnetization loop are presented in Fig. 4. Recorded Fresnel (underfocus) images were constructed also to a video (Video 1). When the field strength was increased to ~0.03–0.05 T, the first domain wall movements were observed: domain walls perpendicular and parallel to the martensite laths moved. According to Freeman and Choi [18], because of anisotropy, the direction of magnetization favors certain crystallographic orientations. Beale et al. [3] noticed that domain walls moved parallel to the martensite/bainite laths in the applied magnetic fields stretching between the laths. In our study, with the increasing field strength, domain walls were observed to stop in the area with thin laths, i.e., to the areas with a high dislocation density. A saturation point was challenging to determine due to these very small and stable domains. However, with the field strength of ~0.25–0.3 T, the saturation was almost achieved. Still, the field strength was increased up to ~0.4 T as in the real BN measurement and the saturation was certainly achieved. When the field strength was decreased from ~0.4 to ~0.1-0.2 T, the first domain walls were observed at the same places as the last ones before the saturation. With the field strength of ~0.02–0.06 T, more domain walls appeared. Thus, it seemed that dislocations were strong pinning sites compared to for example lath boundaries in the same block (low-angle boundary). According to Byeon and Kwun [15], the dislocations have stress fields around them which pin the domain wall motion. In the martensite sample, the residual magnetization was observed; domain morphology changed from the magnetization loop to loop.

3.3.2. Pearlite-ferrite sample

As discussed later in the chapter 3.4, most of the BN emission collected from the pearlite-ferrite sample originates from the ferrite phase and the contribution of pearlite is shadowed. The TEM images (in-focus and Fresnel images) at the initial stage and a few Fresnel (underfocus) images showing the domain wall movements during one magnetization loop in the pearlite-ferrite sample, concentrating on the ferritic structure, are presented in Fig. 5. Recorded Fresnel (underfocus) images were constructed to a video (Video 2). Behavior of ferrite during different magnetization loops was similar to each other. The first domain wall movements were observed when the field strength was increased to ~0.01 T. The walls moved easily inside the ferrite grain due to the small amount of pinning sites. Ferrite/ferrite grain boundaries hindered the domain wall movement, however, domain walls moved also through the grain boundaries. The saturation of ferrite was observed at the field strength of ~0.1 T. Domain walls still existed at ferrite/pearlite boundaries being very strong pinning sites. Domain walls mainly stopped to these boundaries and in some cases, they moved back to inside the ferrite grain. It is really challenging to prove if the domain walls can move through the ferrite/pearlite boundaries or not. The field was increased up to ~0.4 T and when it was decreased back to ~0.1 T, the first walls appeared. When the field strength was decreased to ~0 T, a slight hysteresis was observed; the domain morphology changed slightly compared to the initial stage. Based on the literature [40], soft magnetic materials, can be magnetized by low-strength magnetic fields and only a low residual magnetism exists. The soft magnetic materials are associated also with the low values of magnetic anisotropy [41].

The TEM images (in-focus and Fresnel images) at the initial stage and a few Fresnel (underfocus) images showing the domain wall movements during one magnetization loop in the pearlitic structure are presented in Fig. 6. Recorded Fresnel (underfocus) images were constructed also to a video (Video 3). In pearlite, domain walls perpendicular to ferrite and cementite lamellae start to move at first with a field strength of ~0.02 T. They moved perpendicular to the lamellae. It seemed that cementite hindered slightly more the movement of the domain walls than ferrite lamellae because

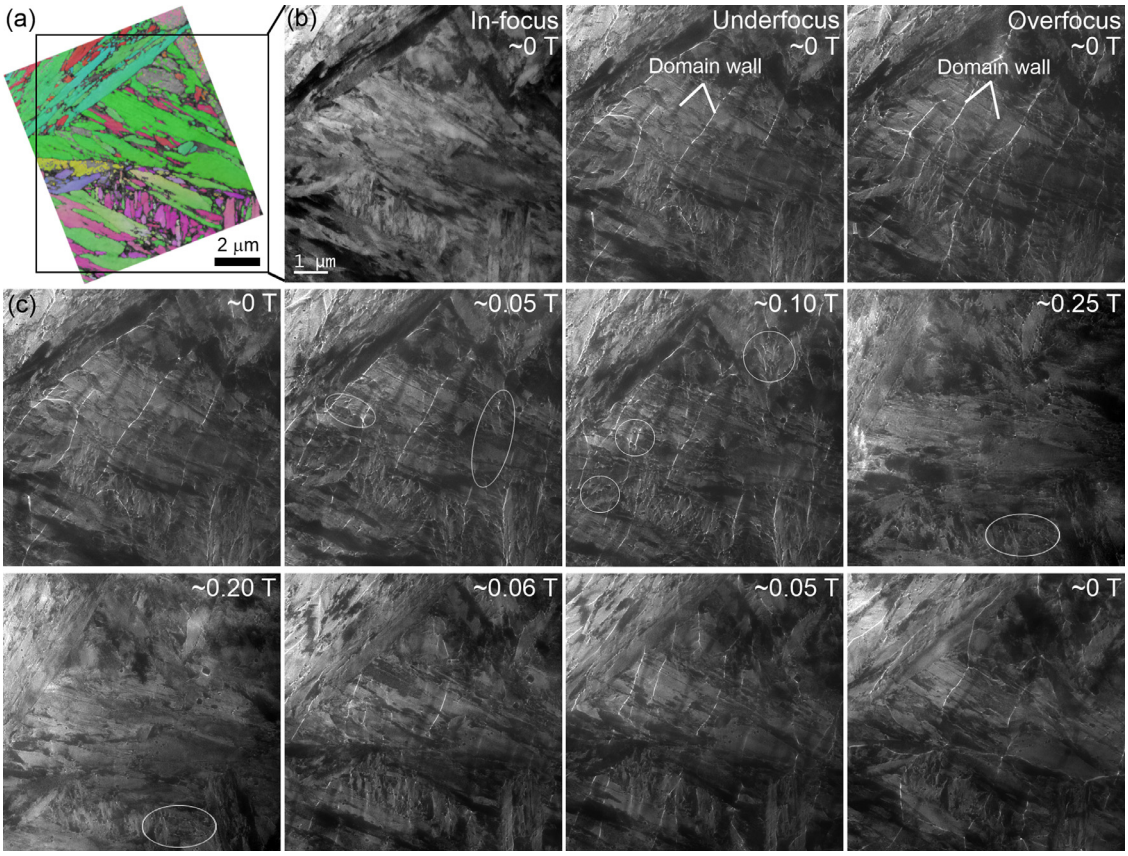

Fig. 4. Visualization of BN measurement by *in-situ* TEM with martensite sample, (a) BC map superimposed with IPF map (IPF color key in Fig. 1c) collected by TKD technique from the area studied, (b) initial stage (in-focus and Fresnel images), and (c) a few Fresnel (underfocus) images from one magnetization loop; inside ellipses, there are changes compared to the previous image.

the walls bent in the cementite lamellae. When the strength of the field was increased to ~0.04 T, also the walls parallel to the ferrite and cementite lamellae moved. Even if the field strength was increased up to ~0.1 T, some domain walls parallel to the lamellae still existed. The field strength of ~0.13 T seemed to be a saturation point. In some areas, there existed small, stable domains between cementite lamellae similar to the small domains in the martensite sample. The field strength was increased up to ~0.4 T as in the actual BN measurement. When the field strength was decreased from ~0.4 to ~0.1 T, the first walls parallel to the lamellae were observed at the same places as the last ones before the saturation. The field strength was decreased to ~0.05 T and the first walls perpendicular to the ferrite and cementite lamellae appeared. When the field strength was decreased to ~0 T, the residual magnetization existed; the domain morphology was slightly different compared to the initial stage. The behavior of pearlite was very similar in all magnetization loops. Saquet et al. [42], Lo et al. [43], and Hetherington et al. [44] found that if the cementite lamellae were parallel to the domain wall, they were stronger pinning sites than lamellae perpendicular to the domain wall. Clapham et al. [4] stated that Fe_3C is ferromagnetic in nature but is nevertheless considered to behave as a nonmagnetic inclusion in the steel matrix acting as a strong obstacle for the domain walls. Neslusan et al. [13] assumed that in the case of Fe_3C, the domain walls are very difficult to unpin by the magnetic field generated with commercial BN sensors and therefore the BN outcome originates only from ferrite. However, we observed that the domain walls pinned by Fe_3C unpinned with the field strength values below the values used in the actual BN measurements.

3.4. Explaining BN outcome by combining BN measurement data and electron microscopy studies

Here, we concentrated on the microstructural steel features affecting the BN outcome. Possible internal stresses especially in the martensitic structure were not separated from the microstructure. In addition, we did not study the effect of 90 and 180° domain walls. Bozorth [45] noticed that 90° domain walls need more energy to move than 180° walls. It has to be noted that the measurement scale of the BN and TEM methods is totally different. In addition, the TEM sample is very thin (< 100 nm) and the BN sample is bulk. However, by visualizing the domain wall movement, we could explain the similarity of the BN outcome from the martensite and pearlite-ferrite samples.

Based on the BN peak positions, the domain wall motion exists with lower magnetic field strengths in the ferrite-pearlite sample than martensite sample (Table 2). According to our *in-situ* TEM studies, the martensitic structure needed the higher field strength (~0.03–0.05 T) to move the domain walls than the ferritic (~0.01 T) and pearlitic (~0.02–0.04 T) structure. In the martensite sample, domain walls perpendicular and parallel to laths started to move with the same field strength value. In the pearlite sample, the walls perpendicular to ferrite and cementite lamellae started to move before the parallel ones (~0.02 T vs. ~0.04 T). The combination of microstructures in the ferrite-pearlite sample and their different domain wall motion behavior causes different shape of the RMS envelope compared to the martensite sample (Fig. 3). The RMS envelope of the ferrite-pearlite sample starts earlier than that of the martensite sample due to soft ferrite. Magnetically harder pearlite may cause “tail” and the envelope of ferrite-pearlite ends

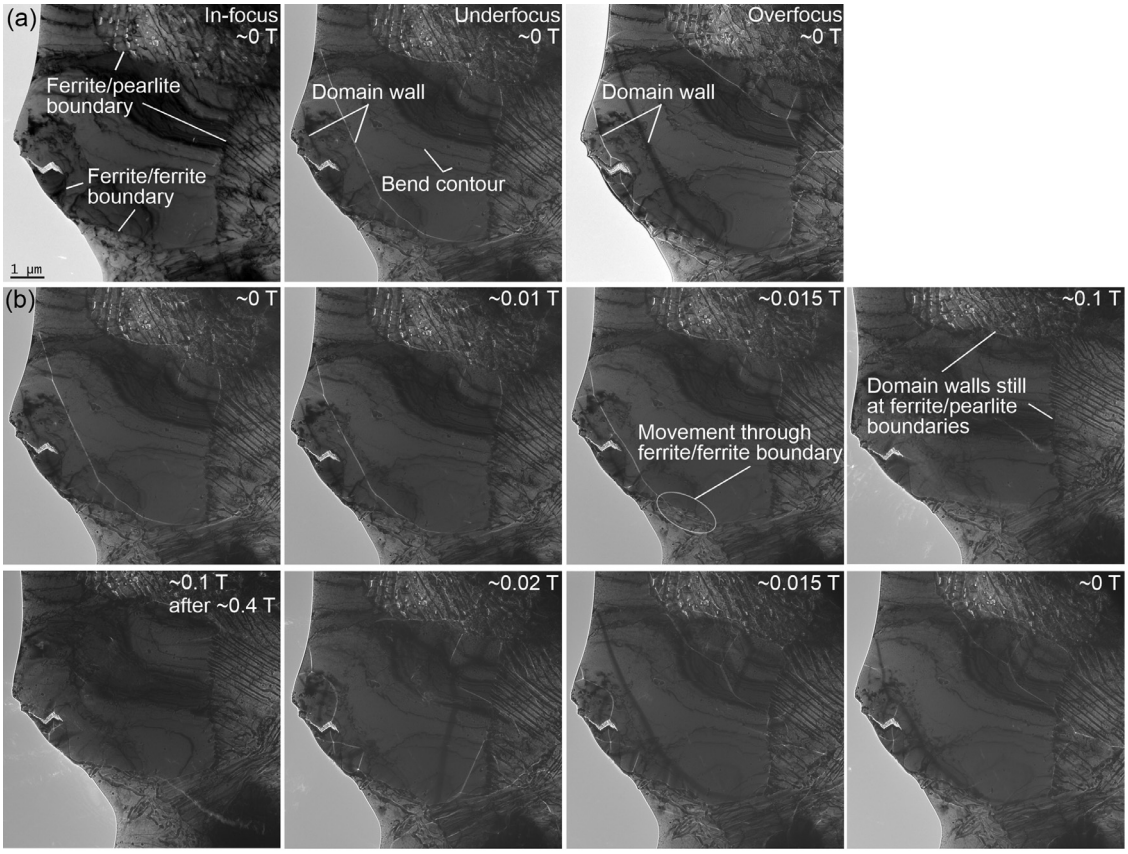

Fig. 5. Visualization of BN measurement by *in-situ* TEM with ferritic structure, (a) initial stage (in-focus, and Fresnel images) and (b) a few Fresnel (underfocus) images from one magnetization loop.

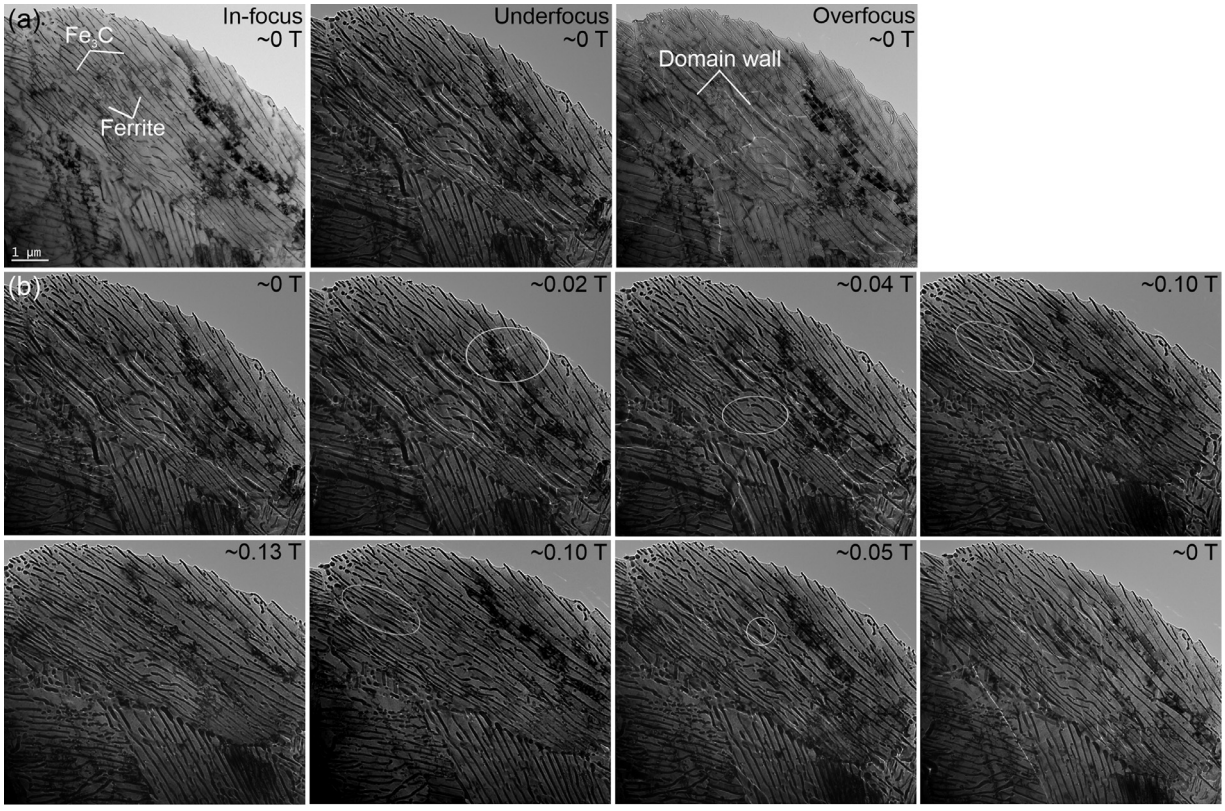

Fig. 6. Visualization of BN measurement by *in-situ* TEM with pearlitic structure, (a) initial stage (in-focus, and Fresnel images) and (b) a few Fresnel (underfocus) images from one magnetization loop; inside ellipses, there are changes compared to the previous image.

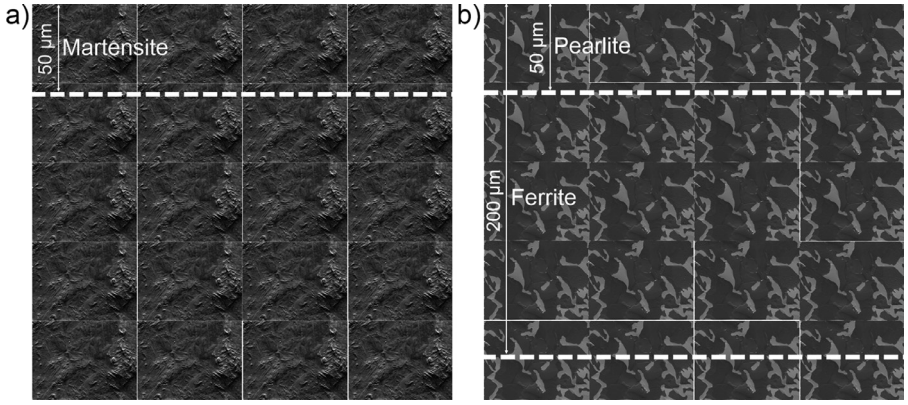

Fig. 7. Graph presenting BN reading depth in different microstructures based on the studies by Stupakov et al. [30,31]. (a) In the martensitic structure the depth is ~50 µm and (b) in the ferritic-pearlitic structure it is in ferrite (bright areas) ~200 µm and in pearlite (dark areas) ~50 µm.

almost at the same time with the envelope of hard martensite. The "humped profile" of the RMS envelope collected from the transitional ferrite-pearlite zone was also noticed by Stupakov et al. [31] similarly to our studies (Fig. 3). However, the peak width values of ferrite-pearlite and martensite were similar (Table 2) but the "tail" in the RMS envelope of the ferrite-pearlite sample is hardly influencing it because the FWHM is calculated as full width at half maximum.

The pulse count was quite close to each other for martensite and ferrite-pearlite despite of their different microstructure. Based on the literature, more pinning sites create higher pulse counts [14]. The relation between pulse count and number of pinning sites is however expected to be complicated due to several features of BN, especially the fact that domain walls move in scale-free avalanches where collective dynamics of a large number of domain wall segments is important [46,47], implying that domain walls might collectively overcome several pinning sites in a given BN jump. According to Stupakov et al. [30,31], the BN reading depth of ferrite is roughly four times more than that of martensite and pearlite. Fig. 7 presents the difference in the BN information depth between the martensite and ferrite-pearlite samples: in martensite and pearlite it is ~50 µm and in ferrite even ~200 µm [30,31]. Martensite has high dislocation density thus lot of strong pinning sites. Pearlite has also strong pinning sites, cementite lamellae. However, their density is not as high as dislocation density in martensite. Ferrite has strong pinning sites only at low incidence, but huge BN information volume compared to martensite and pearlite. One might expect that the lower pinning site density in ferrite is compensated by its larger BN information volume, and hence it seems reasonable that we observe quite similar pulse counts for the martensite and ferrite-pearlite samples.

Based on our findings combining the BN outcome and the microstructural details, it is highly important that the users of the BN method know the microstructure which they assume to be measuring with BN. The BN method is outstanding to point out for example the grinding induced effects on high hardness martensite with tempering grinding burns but could lead to results that are hard to interpret as pointed out in this study. Our achieved fundamental understanding on the detailed microstructural correlations to the BN signal opens new possibilities to utilize the BN method in novel industrial quality control applications.

4. Conclusions

Typically, BN is linked directly to the hardness of material. However, the interpretation of the BN results is usually challenging because of the complexity of the outcome signals. In our study, the BN outcome signal from the martensite and pearlite-ferrite samples was similar even if martensite has much higher hardness compared to ferrite-pearlite. To clarify the connection between microstructural features and BN, the movement of domain walls was visualized, and the BN measurement was mimicked by *in-situ* TEM. We achieved the fundamental understanding on how the microstructural features are manifested in the properties of the BN outcome signal. By combining our BN measurement data and electron microscopy studies, it can be concluded that:

- The domain wall motion exists with lower magnetic field strengths in the ferrite-pearlite sample than in the martensite sample. In martensite, domain walls perpendicular and parallel to laths started to move with the same field strength value. In pearlite, the walls perpendicular to lamellae started to move before the parallel ones. In ferrite, the walls moved easily inside the ferrite grains and managed also through the ferrite/ferrite grain boundaries, but ferrite/pearlite boundaries were very strong pinning sites.
- Magnetically harder pearlite causes "the tail" in the RMS envelope of ferrite-pearlite and the envelope ends almost at the same time with that of hard martensite. Nevertheless, we found similar peak width (FWHM) values for ferrite-pearlite and martensite.
- Pinning site density in ferrite-pearlite (Fe_3C lamellae) is not as high as in martensite (dislocations). Ferrite has strong pinning sites only at low incidence, but as known, huge BN information volume compared to martensite and pearlite. These resulted in the similar pulse count from martensite and ferrite-pearlite.
- Our study indicates that it is very important that BN utilizers know the microstructure that they are measuring with BN-based methods. Only separating BN feature in martensite and ferrite-pearlite was the peak position value.

In our further work, we will study the effect of external, applied stresses on the domain wall motion. In addition, we will take into account the effect of the 90 and 180° domain walls as well as various interlamellar spacing in the pearlitic structure. Also, the thickness of the domain walls, their energy, and free path in different microstructures have to be considered. Our aim is also to modify a TEM specimen holder with a Hall sensor to measure more precise magnetic field strength values in the *in-situ* TEM studies.

Declaration of Competing Interest

The authors declare that they have no known competing financial interests or personal relationships that could have appeared to influence the work reported in this paper.

Acknowledgment

Electron microscopy work made use of Tampere Microscopy Center facilities at Tampere University.

Supplementary materials

Supplementary material associated with this article can be found, in the online version, at doi:10.1016/j.actamat.2021.117378.

References

[1] G.C. Cullity, B.D. Graham, Introduction to Magnetic Materials, Wiley-IEEE Press, Vancouver, 2008, doi:10.1002/9780470386323.fmatter.
[2] S.C. Chikazumi, Physics of Magnetism, John Wiley & Sons, 1964 Incorporatedhttps://books.google.fi/books?id=y6e3tQEACAAJ.
[3] A.D. Beale, J.P. Jakubovics, M.G. Hetherington, C.B. Scruby, B.A. Lewis, K.J. Davies, TEM studies of domains and micromagnetic processes in structural steels, J. Magn. Magn. Mater. 104–107 (1992) 365–367, doi:10.1016/0304-8853(92)90836-D.
[4] L. Clapham, C. Jagadish, D.L. Atherton, The influence of pearlite on Barkhausen noise generation in plain carbon steels, Acta Metall. Mater. 39 (1991) 1555–1562, doi:10.1016/0956-7151(91)90242-S.
[5] A. Trillon, F. Deneuville, S. Petit, B. Bisiaux, Magnetic Barkhausen Noise for hardness checking on steel, in: 18th World Conference on Nondestructive Testin g, Durban, South Africa, 2012.
[6] X. Luo, Y. Wang, L. Wang, J. Xie, Y. Zhang, Non-destructive Hardness Measurement of Hot-stamped High Strength Steel Sheets based on Magnetic Barkhausen Noise, Procedia Eng 81 (2014) 1768–1773, doi:10.1016/j.proeng.2014.10.229.
[7] X. Kleber, A. Vincent, On the role of residual internal stresses and dislocations on Barkhausen noise in plastically deformed steel, NDT E Int 37 (2004) 439–445, doi:10.1016/j.ndteint.2003.11.008.
[8] C. Aranas, Y. He, M. Podlesny, Magnetic Barkhausen noise characterization of two pipeline steels with unknown history, Mater. Charact. 146 (2018) 243–257, doi:10.1016/j.matchar.2018.10.006.
[9] F.A. Franco, M.F.R. González, M.F. De Campos, L.R. Padovese, Relation between magnetic barkhausen noise and hardness for jominy quench tests in SAE 4140 and 6150 steels, J. Nondestruct. Eval. 32 (2013) 93–103, doi:10.1007/s10921-012-0162-8.
[10] A. Ktena, E. Hristoforou, G.J.L. Gerhardt, F.P. Missell, F.J.G. Landgraf, D.L. Rodrigues, M. Alberteris-Campos, Barkhausen noise as a microstructure characterization tool, Phys. B Condens. Matter. 435 (2014) 109–112, doi:10.1016/j.physb.2013.09.027.
[11] A. Sahebalam, M. Kashefi, S. Kahrobaee, Comparative study of eddy current and Barkhausen noise methods in microstructural assessment of heat treated steel parts, Nondestruct. Test. Eval. 29 (2014) 208–218, doi:10.1080/10589759.2014.914207.
[12] S. Sunder Singh, A. Subhash Awale, A. Chaudhari, B. Nahak, Monitoring the microstructural changes of heat treated medium carbon steel by Barkhausen noise and hysteresis loop techniques, Mater, Today Proc 26 (2020) 1198–1202, doi:10.1016/j.matpr.2020.02.241.
[13] M. Neslušan, F. Bahleda, M. Moravčík, K. Zgútová, F. Pastorek, Assessment of tendon prestressing after long-term service via the barkhausen noise technique, Materials (Basel) 12 (2019), doi:10.3390/ma12203450.
[14] D.C. Jiles, Dynamics of domain magnetization and the Barkhausen effect, Czechoslov. J. Phys. 50 (2000) 893–924, doi:10.1023/A:1022846128461.
[15] J.W. Byeon, S.I. Kwun, Magnetic Evaluation of Microstructures and Strength of Eutectoid Steel, Mater. Trans. 44 (2003) 2184–2190, doi:10.2320/matertrans.44.2184.
[16] D. Buttle, C. Scruby, Residual Stresses: Measurement using Magnetoelastic Effects, Encycl. Mater. Sci. Technol. (2001) 8173–8180, doi:10.1016/B0-08-043152-6/01465-0.
[17] D.J. Buttle, C.B. Scruby, J.P. Jakubovics, G.A.D. Briggs, Magneto-acoustic and Barkhausen emission: Their dependence on dislocations in iron, Philos. Mag. A. 55 (1987) 717–734, doi:10.1080/01418618708214379.
[18] M.R. Freeman, B.C. Choi, Advances in Magnetic Microscopy, Science 294 (2001) 1484–1488, doi:10.1126/science.1065300.
[19] T. Kasama, R.E. Dunin-Borkowski, M. Beleggia, Electron Holography of Magnetic Materials, in: F. Monroy (Ed.), Holography: Different fields of application, IntechOpen, Rijeka, 2011, doi:10.5772/22366.
[20] A.K. Lindquist, J.M. Feinberg, R.J. Harrison, J.C. Loudon, A.J. Newell, Domain wall pinning and dislocations: Investigating magnetite deformed under conditions analogous to nature using transmission electron microscopy, J. Geophys. Res. Solid Earth. 120 (2015) 1415–1430, doi:10.1002/2014JB011335.
[21] D.-T. Ngo, L.T. Kuhn, In situ transmission electron microscopy for magnetic nanostructures, Adv. Nat. Sci. Nanosci. Nanotechnol. 7 (2016) 45001, doi:10.1088/2043-6262/7/4/045001.
[22] D. Shindo, Z. Akase, Direct observation of electric and magnetic fields of functional materials, Mater. Sci. Eng. R Reports. 142 (2020) 100564, doi:10.1016/j.mser.2020.100564.
[23] J.N. Chapman, M.R. Scheinfein, Transmission electron microscopies of magnetic microstructures, J. Magn. Magn. Mater. 200 (1999) 729–740, doi:10.1016/S0304-8853(99)00317-0.
[24] M. Tanase, A.K. Petford-Long, In situ TEM observation of magnetic materials, Microsc. Res. Tech. 72 (2009) 187–196, doi:10.1002/jemt.20671.
[25] L.A. Rodríguez, C. Magén, E. Snoeck, C. Gatel, L. Marín, L. Serrano-Ramón, J.L. Prieto, M. Muñoz, P.A. Algarabel, L. Morellon, J.M. De Teresa, M.R. Ibarra, Quantitative in situ magnetization reversal studies in Lorentz microscopy and electron holography, Ultramicroscopy 134 (2013) 144–154, doi:10.1016/j.ultramic.2013.06.003.
[26] S. Santa-aho, A. Sorsa, M. Honkanen, M. Vippola, Detailed Barkhausen noise and microscopy characterization of Jominy end-quench test sample of CF53 steel, J. Mater. Sci. 55 (2020) 4896–4909, doi:10.1007/s10853-019- 04284-z.
[27] V.L. Simo-Pekka Hannula, Eero Haimi, Uudistettu Miekk-ojan Metallioppi, Teknologiateollisuus ry, Helsinki, 2020.
[28] V. Moorthy, B.A. Shaw, P. Hopkins, Surface and subsurface stress evaluation in case-carburised steel using high and low frequency magnetic barkhausen emission measurements, J. Magn. Magn. Mater. 299 (2006) 362–375, doi:10.1016/j.jmmm.2005.04.028.
[29] V. Moorthy, B.A. Shaw, J.T. Evans, Evaluation of tempering induced changes in the hardness profile of case-carburised EN36 steel using magnetic Barkhausen noise analysis, NDT E Int 36 (2003) 43–49, doi:10.1016/S0963-8695(02)00070-1.
[30] A. Stupakov, A. Perevertov, M. Neslušan, Reading depth of the magnetic Barkhausen noise. I. One-phase semi-hard ribbons, J. Magn. Magn. Mater. (2020) 513, doi:10.1016/j.jmmm.2020.167086.
[31] A. Stupakov, A. Perevertov, M. Neslušan, Reading depth of the magnetic Barkhausen noise. II. Two-phase surface-treated steels, J. Magn. Magn. Mater. (2020) 513, doi:10.1016/j.jmmm.2020.167239.
[32] N. Eslahi, A. Foi, Joint sparse recovery of misaligned multimodal images via adaptive local and nonlocal cross-modal regularization, IEEE 8th Int. Work. Comput. Adv. Multi-Sensor Adapt. Process. (2019) 111–115.
[33] K.W. Andrews, D.J. Dyson, S.R. Keown, Interpretation of Electron Diffraction Patterns, Adam Hilger LTD, 1971.
[34] International Centre for Diffraction Data, Powder Diffraction File Database (2020) 00-034-0001.
[35] V. Moorthy, S. Vaidyanathan, K. Laha, T. Jayakumar, K. Bhanu Sankara Rao, B. Raj, Evaluation of microstructures in 2.25Cr-1Mo and 9Cr-1Mo steel weldments using magnetic Barkhausen noise, Mater. Sci. Eng. A. 231 (1997) 98–104, doi:10.1016/S0921-5093(97)00040-3.
[36] K. Davut, C.Hakan Gür, Monitoring the Microstructural Changes During Tempering of Quenched SAE 5140 steel by Magnetic Barkhausen Noise, J. Nondestruct. Eval. 26 (2007) 107–113, doi:10.1007/s10921-007-0025-x.
[37] M. Blaow, J.T. Evans, B.A. Shaw, The effect of microstructure and applied stress on magnetic Barkhausen emission in induction hardened steel, J. Mater. Sci. 42 (2007) 4364–4371, doi:10.1007/s10853-006-0631-5.
[38] T. Inaguma, H. Sakamoto, M. Hasegawa, Microstructure dependence of Barkhausen voltage pulse width in steel, J. Appl. Phys. 111 (2012) 063903, doi:10.1063/1.3694017.
[39] D.M. Stewart, K.J. Stevens, A.B. Kaiser, Magnetic Barkhausen noise analysis of stress in steel, Curr. Appl. Phys. 4 (2004) 308–311, doi:10.1016/j.cap.2003.11.035.
[40] D.C. Jiles, Recent advances and future directions in magnetic materials, Acta Mater 51 (2003) 5907–5939, doi:10.1016/j.actamat.2003.08.011.
[41] F. Fiorillo, Characterization and measurement of magnetic materials, Academic Press, San Diego, 2004. https://doi.org/10.1016/B978-012257251-7/50014-9. https://doi.org/10.1016/B978-0-12-257251-7.X5000-X.
[42] O. Saquet, J. Chicois, A. Vincent, Barkhausen noise from plain carbon steels: analysis of the influence of microstructure, Mater. Sci. Eng. A. 269 (1999) 73–82, doi:10.1016/S0921-5093(99)00155-0.
[43] C.C.H. Lo, C.B. Scruby, G.D.W. Smith, Dependences of magnetic Barkhausen emission and magnetoacoustic emission on the microstructure of pearlitic steel, Philos. Mag. 84 (2004) 1821–1839, doi:10.1080/14786430410001663196.
[44] M.G. Hetherington, J.P. Jakubovics, J.A. Szpunar, B.K. Tanner, High-voltage Lorentz electron microscopy studies of domain structures and magnetization processes in pearlitic steels, Philos. Mag. B Phys. Condens. Matter; Stat. Mech. Electron. Opt. Magn. Prop. 56 (1987) 561–577, doi:10.1080/13642818708220163.
[45] R.M. Bozorth, Ferromagnetism, Van Nostrand, New York, 1951.
[46] P. Cizeau, S. Zapperi, G. Durin, E.H. Stanley, Dynamics of a ferromagnetic domain wall and the barkhausen effect, Phys. Rev. Lett. 79 (1997) 4669–4672, doi:10.1103/PhysRevLett.79.4669.
[47] G. Durin, S. Zapperi, Scaling exponents for barkhausen avalanches in polycrystalline and amorphous ferromagnets, Phys. Rev. Lett. 84 (2000) 4705–4708, doi:10.1103/PhysRevLett.84.4705.